Fabrication of air-bridged Kerr nonlinear polymer photonic crystal slab structures in near-infrared region

Ziming Meng (蒙自明), Xiaolan Zhong (钟晓岚), Chen Wang (王 晨), and Zhiyuan Li (李志远)*

Laboratory of Optical Physics, Institute of Physics, Chinese Academy of Sciences, Beijing 100190, China

**Corresponding author: lizy@aphy.iphy.ac.cn*

Received April 21, 2012; accepted May 28, 2012; posted online September 28, 2012

Fabrication details of air-bridged Kerr nonlinear polymer photonic crystal slab structures are presented. Both the two-dimensional photonic crystal slab and the one-dimensional nanobeam structures are fabricated using direct focused ion beam etching and subsequent wet chemical etching. The scanning electron microscopy images show the uniformity and homogeneity of the cylindrical air holes. The optical measurement in the near-infrared region is implemented using the tapered fiber coupling method, and the results agree with the numerical calculations by using the three-dimensional finite-difference time-domain method.

OCIS codes: 220.4241, 230.5298, 250.5300.
doi: 10.3788/COL201210.112202.

Kerr nonlinear photonic crystals (NPCs) exhibit potential for achieving ultrafast and ultralow power all-optical devices and circuits[1−6]. In recent years, highly nonlinear polymer and nanocomposite polymer materials have outperformed semiconductor materials in terms of large Kerr coefficient and ultrafast response speed[3,4,7]. Although the fabrication methods for high-quality three-dimensional (3D) polymeric PCs have greatly improved in the recent years[8,9], the appropriate technique for fabricating polymeric NPC slab structures remains at its initial stages. Two-dimensional (2D) polymeric PC slab structures have been built using the direct electron-beam lithography technique, which, however, is inevitably restricted in electron beam-sensitive polymers[10]. Subsequently, fabrication of high-quality 2D polymeric NPC by using a combination of electron-beam lithography and reactive ion etching has been proposed[11]. Nanoimprint lithography and wet chemical etching have also been used for fabricating air-suspended 2D polystyrene (PS) PC slab waveguides[12]. However, the fabrication methods mentioned above are time-consuming because they involve multiple processing steps. A fast and direct fabrication method by using focused ion beam (FIB) milling has recently been proposed, and both 2D polymeric PC and 2D polymeric PC microcavities have been successfully constructed[13,14].

During FIB etching, air hole arrays are drilled directly onto the polymeric thin film by using heavy ion bombardment, such as Ga^+ ion, without requiring the use of a mask or a mould. Ultrafast and low-power all-optical switching has been demonstrated in 2D PS PC microcavities fabricated using FIB etching[13]. Most 2D polymeric PC slab structures have been laid on substrate materials with relatively low refractive index, such as silica. However, the small refractive index contrast between the polymer slab and silica substrate is unsuitable for high-Q microcavities because it largely limits the potential application of highly nonlinear polymer materials. We recently proposed an all-optical logic gates scheme based on 2D air-bridged high-Q polymeric PC microcavities[15]. Thus, an appropriate fabrication method for air-bridged polymeric PC slab structures, especially in the near-infrared region should be explored. The current study presents the fabrication procedure based on FIB. The samples are examined using scanning electron microscopy (SEM), and the optical measurement is conducted using the tapered fiber-coupling method[16].

The polymers used in this study were PS materials with a normal molecular weight of 8×10^6 (Fluka Chemie Company, Switzerland). Figure 1 shows the schematic of the fabrication procedure. First, the substrate was prepared by depositing a thick silica layer (with thickness of approximately 1 μm) on the silicon surface by using the plasma-enhanced chemical vapor deposition method. The silica membrane was chosen as the sacrificial layer to form the air-bridged structure. Then, the PS layer was placed on top of the silica layer via spin coating. The thickness of the PS layer was controlled by adjusting the rotation time and speed. To obtain good optical confinement in the vertical direction and maintain a single-mode, the PS slab thickness was fixed at 1 to 1.5a, where a represents the lattice constant of the PC pattern[15]. The thickness of the PS slab was controlled in the range of 500 to 800 nm by setting the photonic band gap (PBG) in the near-infrared region. Two layers of silica and gold with thicknesses of 50 and 100 nm, respectively, were deposited on top of the PS slab prior to FIB etching. The gold layer was used for

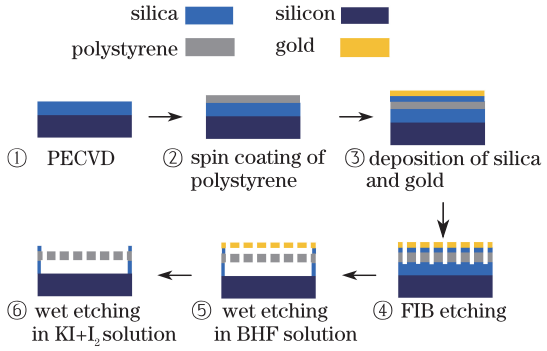

Fig. 1. (Color online) Schematic illustration of the fabrication procedure.

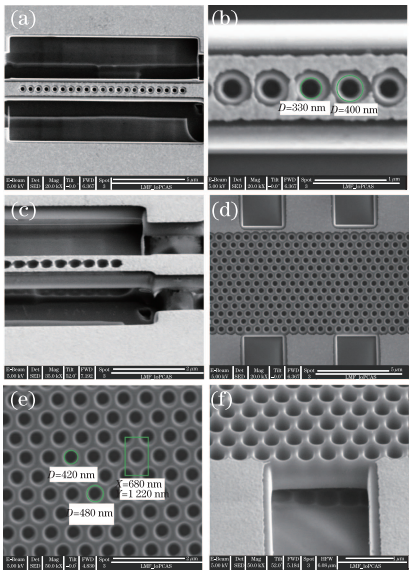

Fig. 2. SEM images of the fabricated samples. (a)–(c) SEM images of the 1D air-bridged PS nanobeam structures. (d)–(f) SEM images of the 2D air-bridged PS slab structures. The diameters of the fabricated holes and the lattice constant of the PC structures are marked in (b) and (e). The designed cylindrical hole has a tendency to transform into a small cone shape in the practical samples. The samples in (c) and (f) are tilted at an angle of 52°. The topmost gold layer is not removed to obtain clear and stable SEM images.

the charge removal during the FIB etching process, and the silica layer contributed to the complete removal of the gold layer in the final wet chemical etching step. The FIB system (Model DB235, FEI Company, USA) was used to prepare the periodical patterns in the PS layer. By simultaneously considering fabrication time and precision, an appropriate spot current of 100 pA was used to drill the air hole arrays. The cylindrical air holes were cut through the PS layer down to the silica substrate. The samples were immersed in the buffered hydrofluoric acid (BHF) to etch the underlying silica layer and form the air-suspended PC slab. The immersion time was precisely controlled to fully remove the silica layer underneath the hole arrays. Finally, the top gold layer was removed by dipping the sample in the KI and I_2 mixed solution.

Figure 2 shows the SEM images of the fabricated samples, wherein the topmost gold layer was reserved to obtain clear and stable SEM images. Both the conventional 2D air-bridged PS PC slab and the one-dimensional (1D) nanobeam structures were successfully fabricated. As can be seen in Fig. 2, the fabricated air hole arrays are uniform and homogeneous. The hole diameters marked in Figs. 2(b) and (e) are approximately 330 and 430 nm for the 1D nanobeam structures and 2D triangular lattice PC, respectively. Considering that the aspect ratio between the slab thickness and the hole diameter reached 2:1, the tendency of the designed cylindrical hole to transform into a small cone shape is unavoidable in practical samples. An obvious air gap with thickness of approximately 1 μm are observed when the samples are tilted at an angle of 52°, as shown in Figs. 2(c) and (f).

Two PS strip waveguides adjacent to the hole arrays were fabricated to couple light in and out of the PC structures and examine the optical performance of the fabricated PC structures. The PS waveguides had widths of approximately 4 μm, which was formed by etching two nearby air trenches with a width of 3 μm, as shown in Fig. 2(d). However, the input and output ends of the PS waveguides were slightly lifted off the substrate after being immersed in the BHF despite the intactness of the PC structures because of the over-etching of the underlying silica layer of the waveguide region, as shown in Fig. 3. In this circumstance, the coupling between the tapered fiber and waveguide is too weak to detect the output signal. Thus, to measure the transmission spectrum, the waveguide butt should be protected by coating it with some acid-proof materials or a different coupling scheme that does not use narrow input and output strip waveguides, such as the prism coupling or curved microfiber coupling method, should be used[13,17]. Although the transmission spectra of the air-bridged PC are currently out of reach, the quality of the fabricated structures is believed to be high, as proven in the SEM images that indicate the feasibility of the fabrication method.

The effective refractive index of the substrate materials becomes largely reduced when the air hole into the substrate is sufficiently deep. Similarly, the situation is close to the air-bridged condition[18]. Thus, instead of completely removing the silica layer underneath using wet chemical etching, the air hole is deeply etched into the silica layer with a depth of a. The 3D finite-difference time-domain (FDTD)[19] method was used to simulate the transmission spectra of a 2D square lattice PC structure with an air hole deep into the substrate. The chosen TE polarization (the electric field in the slab plane) is likely to have large PBG effect on the hole patterns. The radius of the air hole and the thickness of the slab were $0.3a$ and $1.5a$, respectively. The depth of the air hole in the silica substrate was set as a. The lattice constant a was chosen to be 530 nm to set the PBG edge in the near-infrared region. Figure 4(b) shows the simulated results from the transmission spectrum along the x-axis direction of the PC structure, where the PBG edge was clearly maintained in the range of 1 450 to 1 650 nm.

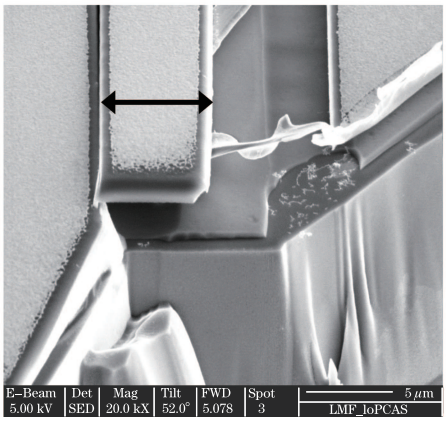

Fig. 3. SEM image of the input or output end of the PS waveguides. The input or output waveguide is marked by a black double arrow. The sample is tilted at an angle of 52°. The topmost gold layer is not removed to obtain a clear and stable SEM image.

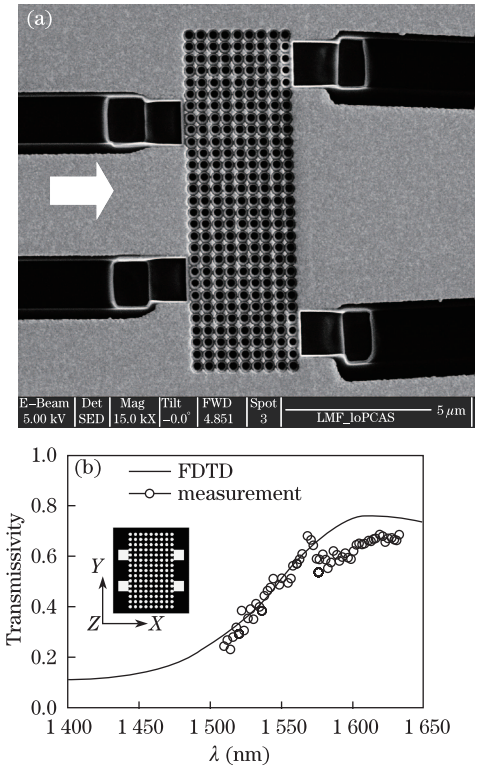

Fig. 4. SEM image of the fabricated square lattice PC structure with a deep air hole in the substrate. The topmost gold layer was not removed to obtain a clear and stable SEM image. The arrow represents the propagation direction. (b) 3D FDTD simulated result and the optical measurement result obtained using the tapered fiber coupling method. The inset shows the schematics of the simulated PC pattern, where the black and white regions represent the PS and the air, respectively.

We built the structure according to the simulation parameters by using the fabrication procedure discussed above, but without the BHF etching step. Figure 4(a) shows the SEM image of the fabricated structure. Two PS strip waveguides were placed in the two sides of the PC pattern for light coupling. To enhance the output signal, the width of the output waveguide butt adjacent to the PC structure was enlarged and then tapered to 4 μm at the output end. The input optical signal from a continuous wave tunable semiconductor laser with a wavelength in the range of 1 500 nm to 1 640 nm was launched into the facet of the input strip waveguide via a single-mode tapered fiber. The polarization of the optical signal was adjusted to TE polarization prior to the application of the input strip waveguide. The signal from the output strip waveguide was collected using another single-mode tapered fiber and then sent to the power meter for recording. Figure 4(b) shows the measured result obtained after correction for the loss from the interface between PS and air. The simulated and measured results were in good agreement with each other, indicating the high quality of the structure and the feasibility of the fabrication method.

In conclusion, the fabrication procedure for air-bridged PS PC slab structures is discussed. Both the conventional air-bridged 2D PS PC slab and the 1D nanobeam structures are successfully fabricated. The air hole arrays are uniform and homogeneous, and an obvious air gap is obtained, as shown in the SEM images. Although the PC slab is intact and complete, the connecting planar waveguide end is slightly lifted off of the substrate because of the over-etching in the BHF, indicating that the measurement by using the in-plane waveguide is inappropriate during this stage. The PC pattern with a deep air hole in the silica substrate is investigated to examine the transmission spectrum. The square lattice PC slab structure is fabricated, and the measured result agrees with the numerical result calculated using the 3D FDTD method. The results of this study indicate the potential of FIB as a direct fabrication method for the construction of highly nonlinear all-optical devices and circuits.

This work was supported by the National Basic Research Foundation of China (No. 2011CB922002) and the Knowledge Innovation Program of Chinese Academy of Sciences (No. Y1V2013L11).

References

1. M. Scalora, J. P. Dowling, C. M. Bowden, and M. J. Bloemer, Phys. Rev. Lett. **73,** 1368 (1994).
2. R. E. Slusher and B. J. Eggleton, *Nonlinear Photonic Crystals* (Springer, Berlin, 2003).
3. Y. Liu, F. Qin, Z. Y. Wei, Q. B. Meng, D. Z. Zhang, and Z. Y. Li, Appl. Phys. Lett. **95,** 131116 (2009).
4. Y. Liu, F. Qin, F. Zhou, Q. B. Meng, D. Z. Zhang, and Z. Y. Li, Front. Phys. China **5,** 220 (2010).
5. K. Nozaki, A. Shinya, S. Matsuo, Y. Suzaki, T. Segawa, T. Sato, Y. Kawaguchi, R. Takahashi, and M. Notomi, Nature Photon. **6,** 248 (2012).
6. J. D. Cox and M. R. Singh, J. Appl. Phys. **108,** 083102 (2010).
7. M. R. Singh and R. H. Lipson, J. Phys. B: At. Mol. Opt. Phys. **41,** 015401 (2008).
8. Z. Y. Zheng, X. Z. Liu, Y. H. Luo, B. Y. Cheng, D. Z. Zhang, Q. B. Meng, Wang, and Y. R. Wang, Appl. Phys. Lett. **90,** 051910 (2007).
9. H. Dong, J. Gao, X. Kong, M. Cai, and L. Shi, Chin. Opt. Lett. **5,** 580 (2007).
10. R. R. Panepucci, B. H. Kim, V. R. Almeida, and M. D. Jones, J. Vac. Sci. Technol. B **22,** 3348 (2004).
11. J. H. Wülbern, M. Schmidt, U. Hübner, R. Boucher, W. Volksen, Y. Lu, R. Zentel, and M. Eich, Phys. Stat. Sol. **204,** 3739 (2007).
12. C. G. Choi, Y. T. Han, J. T. Kim, and H. Schift, Appl. Phys. Lett. **90,** 221109 (2007).
13. X. Y. Hu, P. Jiang, C. Y. Ding, H. Yang, and Q. H. Gong, Nature Photon. **2,** 185 (2008).
14. E. Pialat, T. Trigaud, J. P. Moliton, and M. Thévenot, J. Polym. Sci. B Polym. Phys. **45,** 2993 (2007).
15. Y. Liu, F. Qin, Z. M. Meng, F. Zhou, Q. H. Mao, and Z. Y. Li, Opt. Express **19,** 1945 (2011).
16. L. Gan, C. Z. Zhou, C. Wang, R. J. Liu, D. Z. Zhang, and Z. Y. Li, Phys. Status Solidi. A **207,** 2715 (2010).
17. K. Srinivasan, P. E. Barclay, M. Borselli, and O. Painter, Phys. Rev. B **70,** 081306 (2004).
18. G. Böttger, M. Schmidt, M. Eich, R. Boucher, and U. Hübner, J. Appl. Phys. **98,** 103101 (2005).
19. A. F. Oskooi, D. Roundy, M. Ibanescu, P. Bermel, J. D. Joannopoulos, and S. G. Johnson, Comput. Phys. Commun. **181,** 687 (2010).